RESPONSE OF THE CUTOFF RIGIDITY OF COSMIC RAYS TO CHANGES IN THE DYNAMIC AND MAGNETIC PARAMETERS OF THE SOLAR WIND AND GEOMAGNETIC ACTIVITY DURING THE STORM ON MARCH 23–24, 2023

© 2025 Ptitsyna N.G., Danilova O.A., Tyasto M.I.

Pushkov Institute of Terrestrial Magnetism, Ionosphere and Radio Wave Propagation, St. Petersburg Branch, Russian Academy of Sciences, St. Petersburg, Russia

**e-mail: md1555@mail.ru*

Received January 16, 2025

Revised January 21, 2025

Accepted April 14, 2025

Abstract. We investigated the correlations between the cutoff rigidity of cosmic rays and the parameters of interplanetary space, solar wind, and geomagnetic activity during a strong magnetic storm on March 23–24, 2023. The cutoff rigidity of cosmic rays was obtained by calculating the trajectories of particles in the magnetic field of the solar wind according to the Tsyganenko Ts01 model. The analysis showed that the changes in the cutoff rigidity is controlled mainly by changes in the indices of geomagnetic activity *Dst* (correlation coefficient $k \approx 0.95$), as well as electromagnetic parameters — the total value of the interplanetary magnetic field *B*, its component *Bz*, the azimuthal component of the electricfield *Ey* and the plasma parameter β ($|k| \approx 0.6$–0.75). The parameters of the solar wind such as velocity V, density N, and dynamic pressure P have little effect on the variations of the cosmic ray cutoff rigidity ($|k| < 0.45$).

Keywords: *cosmic ray cutoff rigidities, cosmic rays, solar wind, magnetic storm, interplanetary magnetic field, geomagnetic activity*

DOI: 10.31857/S00167940250403e6

1. INTRODUCTION

The Earth's magnetic field is a natural shield for flows of energetic charged particles bombarding the Earth from outer space, in particular, galactic cosmic rays (GR). The possibility of penetration of charged particles inside the magnetosphere is determined by their magnetic stiffness R (moment per unit charge). Since particles with the same stiffness move along the same trajectories in a constant magnetic field, stiffness is often used to study geomagnetic shielding. At a fixed time at a given point in time, geomagnetic clipping stiffness R_c is a threshold value, and only particles with stiffnesses higher than this threshold can reach the Earth's atmosphere. The effective clipping stiffnesses R_{ef} represent the average shielding effect, accounting for all possible angles of particle incidence, although in practice, because of the cumbersome nature of such calculations, only vertical directions are often calculated unless a special task is assigned. Calculations of the geomagnetic clipping stiffness began with the pioneering work of Størmer [1955], where only the dipole component of the geomagnetic field was taken into account in the theoretical analysis. Nowadays, the standard method for obtaining R in the Earth's magnetic field is numerical integration of the equation of motion of charged particles in the geomagnetic field, which is described by some model. Both dipole and non-dipole components are considered. This method was developed in the 1960s [McCracken et al., 1962; Shea et al., 1965], and since then, numerous studies of magnetospheric effects in CL variations have been widely carried out on its basis [e.g., Kress et al., 2010, 2015; Belov et al., 2021 and references therein].

The geomagnetic field is constantly changing on different time scales, which causes corresponding changes in the interaction of the magnetic and electric fields of the solar wind (SW) with the fields and currents in the magnetosphere and determines changes in the magnetic shielding. Particularly significant changes in magnetospheric shielding are observed during magnetic storms. At this time, global current systems are formed in the magnetosphere: ring current, magnetopause current, magnetospheric tail currents, and high-latitude longitudinal currents. These currents reduce the field strength inside the magnetosphere, thereby weakening the magnetic shielding, i.e., variations of the geomagnetic clipping stiffness ΔR_{ef} are observed. Variations in the stiffnesses of the geomagnetic clipping of CL lead to redistribution of the fluxes of charged particles in the magnetosphere and, as a consequence, to changes in the intensity of the fluxes reaching the Earth's surface [Dorman, 1963].

During a magnetic storm, solar wind energy is transferred to the Earth's magnetosphere by coronal solar mass ejections (CMEs) or high-speed corotating flows from coronal holes. The strongest geomagnetic storms (Dst < -100 nTL) are caused mainly by transient events - CMEs and related

interplanetary structures (shock fronts, compression regions in front of interplanetary *CMEs*, magnetic clouds, and magnetic "pistons") [Gosling 1993; Gonzalez et al., 1999; Ermolaev et al., 2009; Richardson, 2018]. The response of geomagnetic shielding to changes in the geomagnetic environment, the NE and the interplanetary magnetic field (IMF) during magnetic storms is poorly understood, despite a number of studies in this area [Belov et al., 2005; Shimazu, 2009; Tyssøy and Stadsnes, 2014; Kress et al., 2010; Ptitsyna et al., 2019].

The purpose of this study is to determine the geomagnetic thresholds R_{ef} during a strong magnetic storm on March 23-24, 2023, and to analyze the dependence of their changes ΔR_{ef} on the parameters of the interplanetary medium and geomagnetosphere.

2. METHOD AND DATA

The vertical effective geomagnetic thresholds R_{ef} were numerically calculated for March 23-24, 2023 through the determination of particle trajectories in the magnetic field of the Tsyganenko Ts01 magnetospheric model ([Tsyganenko et al., 2003] and references therein). In this case, the accuracy of the determination of geomagnetic thresholds depends on the accuracy of the magnetospheric model used in the calculations. According to the Ts01 model, the magnetic field inside the magnetosphere (without the main magnetic field) is the sum of contributions from the main magnetospheric current systems. The current systems were parameterized using satellite data measured during 37 geomagnetic storms with $Dst \leq$ -65 nTL [Tsyganenko et al., 2003]. The Ts01 model includes Chapman-Ferraro currents that constrain the Earth's magnetic field inside the magnetospheric boundary, symmetric and partial bulk circular currents, transverse tail currents, and large-scale longitudinal currents. To constrain the field inside the magnetosphere, a block was included to describe the interaction field, which represents the effect of the interplanetary magnetic field penetrating inside the magnetosphere. The interaction field is represented as a homogeneous magnetic field that is proportional to and directed along the transverse component. For calculations of the magnetic field from internal sources, the representation of the Earth's main magnetic field (EMF) as a series expansion over spherical harmonic functions up to $n = 10$ is used. In the Ts01 model, the *Dst variation*, the density N and velocity V *of* the NE, and the MMP components By and Bz are used as input parameters. Calculations were performed for each hour with respect to the mean geomagnetic clipping stiffnesses during quiet time on March 12, 2023, for nine stations, which were chosen to cover the main region of the R_c threshold stiffnesses affected by the geomagnetic field during quiet time. The data on the stations are presented in Table 1.
Table 1.

Further, the correlation coefficients k and standard errors s of variations of the geomagnetic clipping stiffnesses ΔR_{ef} were calculated with the following parameters: the Bz and By components and the total IMF value B, the azimuthal component Ey of the electric field, the plasma parameter β, the velocity V, density N and pressure P of the NE, and the geomagnetic activity indices Dst and Kp. These parameters are taken from the OMNI database at https://omniweb.gsfc.nasa.gov/form/dx1.

Plasma β is the ratio of plasma pressure to magnetic pressure; in the OMNI database this parameter is calculated by the formula

$\beta = (4.16T/10+5.34)\times Np/B^2$, where

T in degrees Kelvin; Np in cm^{-3}; B in nTl.

The electric field was calculated by the formula

$E\ V\ Bz = -\times\times 10^{-3}$, where E in mV/m; V in km/s; Bz in nTl.

The coefficients k and errors s are obtained from the correlation analysis applied to the magnetic storm from 0:00 UT 23 to 23:00 UT March 24, 2023 (day of year DOY 82 and 83).

2. MAGNETIC STORM ON MARCH 23-24, 2023 AND VARIATIONS OF GEOMAGNETIC THRESHOLDS

Figure 1 shows the magnetic and dynamical parameters of the solar wind and geomagnetic activity during the geomagnetic storm of March 23-24, 2023; the azimuthal component Ey of the electric field, the total interplanetary magnetic field (IMF) B, the Bz and By components of the IMF, the plasma parameter β, velocity V, density N, pressure P *of* the NE, and the geomagnetic activity indices Dst and Kp are given from top to bottom.

Fig. 1.

This was the first strong geomagnetic disturbance that occurred when approaching the maximum of the current 25th solar cycle in October 2024. The peculiarity of this storm in March 2023 was the fact that it was caused by a *stealth coronal mass ejection (*CME) that left the Sun on March 20, 2023. Stealth CMEs have a number of remarkable features, in particular they are characterized by low velocity. Such *CMEs* are not associated with any visible manifestations on the Sun, so they are difficult to identify and predict their geoeffectiveness. In particular, the CME that initiated the studied geomagnetic storm was missed by all observers and not listed as a CME (https://kauai.ccmc.gsfc.nasa.gov/CMEscoreboard/PreviousPredictions/2023) because the CME's sliding effect on the Earth's magnetosphere was initially predicted. Therefore, the impact of this *CME* was not expected to be geoeffective. However, because the peak value of the storm index *Dst*

unexpectedly reached -163 nTL, this storm was qualified by the National Oceanic and Space Administration (NOAA) as a "strong" storm [Tahir et al., 2024; Teng et al., 2024].

The development of the investigated storm has a complex non-standard character. It is similar to the evolution of a two-stage disturbance, but with a characteristic feature introduced by the fact that this storm was initiated by a hidden source on the Sun, namely, a hidden coronal mass ejection CME. This CME moved at a low velocity, insufficient to form a shock wave, but nevertheless it manifested itself in changes of many NE parameters. As a result of the interaction between such a specific interplanetary disturbance and the magnetosphere, the total IMF magnetic field $|B|$, proton density N, and dynamic pressure P, as well as the southern component of the IMF Bz, gradually increase on March 23 at 07:40-14:20 UT (Fig. 1), which means that the *ICME's sheath region* or CME compression *region* passes near the Earth. At the end of this period at ~13:00 UT (hourly data values are used in this paper), the main phase of the storm began (Dst = -50 nTL), which developed slowly and inexpressively until ~18:00 UT, when its active phase began with a sharp decrease in Dst, which reached its minimum (-163 nTL) at 02:00 UT on March 24, 2024. Thus, the evolution of the main phase occurred at the already formed ring current against the background of low velocity (450-490 km/s) and weak dynamic pressure (~2-3 nPa) of the solar wind [Gromova et al., 2024]. At the same time, the value of *the Bz-component of* the MMP practically did not change for a long time ~11 h, remaining close to~ -15 nTl. Note that a negative value of Bz for a long time (≥3 h) is a necessary condition for the formation of a magnetic storm [Gonzalez and Tsurutani, 1987]. The geomagnetic index Kp began to increase from 03:00 UT and reached the maximum value Kp = 8 during the decline phase at 3:00 UT on the next day on March 24. The Ey variations were similar to the Bz variations, but of the opposite orientation, and reached a peak value of 7.66 mV/m on March 23 at 23:00 UT. As a result, the Dst index, representing the ring current intensity, became negative at ~11:00 UT and then reached a negative peak of -163 nTL at 02:00 UT on March 24, 2023 (DOY 83). After this, the *Dst-index* began to increase, the southern component of the IMF Bz also began to increase, remaining negative all the time, and the magnetic storm entered the relaxation phase.

Fig. 2.

Fig. 2 shows the calculated variations of geomagnetic thresholds ΔR_{ef} for all studied stations during the storm of September 23-24, 2023. To illustrate the connection between the dynamics of geomagnetic thresholds and the evolution of the storm, Fig. *2a* also shows the course of *the* Dst-index. In Figure 2b, the ΔR_{ef} curves are arranged from top to bottom in the order of decreasing threshold stiffnesses R_c (increasing station latitude, except for the KGSN station located in the southern

hemisphere). Figure *2b* shows the decreasing stiffnesses of geomagnetic clipping during the storm, which increases with increasing latitude. Figure 2 shows that ΔR_{ef} reach their minimum values during the storm maximum (*Dst* minimum). It is shown that the maximum decrease of thresholds to $\Delta R_{(ef)} \approx$ -0.8 GV is observed at the stations with higher latitudes MOSC and KGSN at 02:00 UT on March 24 during the storm peak (minimum *Dst* =− 163 nTL). At lower latitudes at the stations ESOI, ATHN, AATA, IRKT (higher rigidity of geomagnetic clipping at quiet time), the decrease of geomagnetic thresholds is less ($\Delta R_{ef} \approx$ -0.3 ÷ -0.5 GW).

Our result confirms previous findings that the rigors of geomagnetic clipping are most strongly suppressed during the maximum of the storm's main phase, when *Dst* reaches its minimum. The response of geomagnetic shielding to changes in conditions in the NE outside the main phase is much less clear by now. In Fig. *2b*, we observe an additional drop in the stiffness ΔR_{ef} well before the storm maximum, at the beginning of the main phase (March 23, at 13:00 UT). In [Kress et al., 2004], using observations and calculations, it is shown that an increase in the dynamic NE pressure *P* suppressed the clipping stiffnesses during the November 24, 2001 storm during the *sudden* storm *commencement ssc* (*sudden storm commencement*). In [Flückiger et al., 1990; Belov et al., 2005] it is shown that the geomagnetic clipping stiffnesses, on the contrary, increase at the beginning of the storm with respect to the level of the quiet field due to the formation of currents on the magnetopause. In [Kress, 2010, 2015] it is indicated that an increase in *P* can cause both an increase and a decrease in the stiffnesses depending on the conditions in the NE and the local time. In the case of the studied storm at the beginning of its main phase, at 13:00 UT at all CL stations (Fig. *2b*), a significant negative jump in ΔR_{ef} values is seen≈ -0.5 GV (i.e., a decrease in ΔR_{ef} values in contrast to the increase found by [Flückiger et al., 1990; Belov et al., 2005]). It is indicated in [Teng et al., 2024] that at this moment a magnetic cloud passage was observed, which in this case was not accompanied by a shock wave and sudden onset of the SSC storm, since the ICME velocity was not high enough. Such peculiarity is characteristic of the hidden CMEs, one of which was the source of the observed strong perturbation in the geomagnetosphere. The maximum decrease of ΔR_{ef} values ≈ -0.5 GW at the beginning of the main phase of the storm is observed for Moscow station. This decrease of variations of the variations of the geomagnetic clipping stiffnesses was significant and comprised ~70 % of the maximum decrease at the *Dst* minimum, i.e., at the storm maximum. The decrease of the geomagnetic clipping stiffnesses before the beginning of the main phase of the storm is a response to a large jump of the dynamic pressure *P* = 14.79 nPa at 12:00 UT, which indicates a sharp compression of the magnetosphere despite the absence of a shock front. However, probably, the dominating influence of the ring current compared to the

currents at the magnetopause caused precisely the decrease of ΔR, similar to the main decrease at the storm maximum.

3. CORRELATION ANALYSIS OF VARIATIONS OF GEOMAGNETIC THRESHOLDS

The time curves of Figs. 1 and 2 show qualitatively how the ΔR_{ef} values respond to changes in the NE, IMF, and geomagnetic activity parameters. In order to quantitatively assess the contribution of the studied interplanetary and geomagnetic parameters to the variations of geomagnetic thresholds, we analyzed the correlations of ΔR values with the studied parameters. Table 2 summarizes the correlation coefficients of ΔR_{ef} values with *Dst, Kp(,)Ey, W, By, B, N, V, P,* and β for the magnetic storm period along with the standard errors *s*. The stations in Table 2 are arranged in the order of decreasing thresholds in quiet time from st. ESOI to st. KGSN, i.e., from 10.73 GV to 1.9 GV.

Table 2.

Table 2 shows that the best correlation of ΔR_{ef} is observed with *Dst* (*k*0.93±0.09÷ 0.96±0.05) with the maximum *k*= 0.96±0.05 for the midlatitude station JUNG. The negative correlation with the geomagnetic index *Kp* is somewhat smaller (*k*-0.74±0.11 ÷ -0.80±0.14), however it is highly significant with a maximum anti-correlation observed at higher latitude stations MOSC (-0.80±0.14) and KING (-0.80±0.15). In addition, significant correlation/anti-correlation is found for all electromagnetic parameters except *By*: *B* (*k*-0.68±0.16 ÷ -0.74±0.16), *Bz* (*k*0.59±0.09÷ 0.7±0.17), *Ey* (*k*-0.57±0.09 ÷ -0.68±0.18), and β (*k*0.57±0.17÷ 0.71±0.12). The correlation for the By *component is* insignificant (*k*0.29±0.23− 0.38±0.20). The results of the correlation analysis show that *k* between the values of ΔR_{ef} and all the dynamic CB parameters (*V, N,* and *P*) is significantly smaller: $|k| \geq 0.45$ at all stations. It should be noted that the calculation errors *s are* small for higher *k* (with the parameters of the electromagnetic field and geomagnetic activity) and increase at low *k* (with the dynamic CB parameters and the B_y-component of the MMP).

The most geoeffective parameters in this work are those for which the correlation/anti-correlation coefficient $|k| \geq 0.45$. For more clarity of the geoeffectiveness of some parameters, Fig. 3 presents the results of calculations of correlations between the values of ΔR_{ef} and the parameters of geomagnetic activity, solar wind, and MMP, for which $|k| \geq 0.45$. Figure 3 demonstrates that such parameters during the March 23-24, 2023 storm were *Dst*, *Kp*, β, *B*, *Ey*, and *Bz*. Thus, we can conclude that the control of the ΔR_{ef} variation values during the evolution of the studied storm was carried out mainly by

the geomagnetic activity dynamics and electromagnetic parameters, while the NE dynamic parameters had almost no influence on the behavior of the clipping stiffnesses.

Fig. 3.

4. DISCUSSION OF RESULTS

In this paper, we quantitatively assessed which geomagnetospheric parameters were the most geoeffective and contributed most to the variations of geomagnetic thresholds on March 23-24, 2023. For this purpose, we analyzed the correlations of ΔR_{ef} values with the parameters of geomagnetic activity, NE, and MMP. It may seem obvious that changes in the values of the effective stiffnesses ΔR_{ef} should have a high degree of correlation with the input parameters of the magnetospheric field model used. In the case of the Ts01 model, these are the *Dst-index*, the density *N* and velocity *V of* the CB, and the Bz *and By-components of* the MMP. However, it should be taken into account that the dependence of ΔR_{ef} values on these input parameters in the Ts01 semiempirical model is not direct, but indirect, through the calculation of particle trajectories in the model magnetic field, which is given by the superposition of different current systems. At the same time, these current systems themselves, their relative contribution to the model magnetic field and, consequently, to the variations of stiffnesses ΔR_{ef} makes this dependence much more complicated. Generally speaking, the description of the magnetospheric magnetic field in terms of accounting for the contributions of various current sources is a rather common approach. Other magnetospheric models such as the paraboloidal model [Alexeev et al., 2001] or the model focused on different individual events [Ganushkina et al., 2018] also describe the observed field variations using combinations of different individual sources [Kalegaev et al., 2005]. Different Tsyganenko models also utilize different relations to account for the different relative importance of the contributions of tail currents and, for example, ring currents for different perturbation conditions in the geomagnetosphere [Kalegaev, 2011; Dubyagin et al., 2014; Castillo et al., 2017]. When studying specific storms using Tsyganenko models, it has been obtained that the correlation of ΔR_{ef} values with the model input parameters can be either high or low [Adriani et al., 2016; Ptitsyna et al., 2019; Ptitsyna et al., 2023]. In particular, the analysis in this paper shows that for the March 2023 storm, a very high correlation coefficient k= 0.93-0.96 is observed for *Dst*. In addition, for *Kp*, which is not an input parameter of the model, a k$\left|\right|$=0.75-0.8 is obtained, that is, a higher degree of correlation is observed than with all other input parameters except *Dst*. Also high correlation is obtained for all electromagnetic parameters except *By*: *B*, *Bz*, *Ey* and β. In contrast, the *k* between the

values of ΔR_{ef} and all dynamic parameters of CB - *V, N*, and *P* - is significantly smaller: $|k| < 0.45$ at all stations.

It is believed that the main role in the development of magnetospheric perturbations is played by the reconnection of the CB magnetic field and the geomagnetospheric field, as well as by the CB dynamic pressure *P* responsible for the compression of the magnetosphere [Dungey, 1961; Russell, 1976; Akasofu, 1984]. Both of these factors weaken the geomagnetic shield, reduce the rigidity of geomagnetic clipping, and facilitate the penetration of NE plasma into the Earth's magnetosphere and atmosphere. Indeed, high correlation coefficients with both B_z and dynamic parameters of the NE and magnetosphere were obtained when studying the correlations between clipping stiffnesses and NE and magnetospheric parameters for various intense storms [see, e.g., Ptitsyna et al., 2019; Danilova et al., 2023]. However, in the case of the storm in March 2023, we obtained that the control of changes in the geomagnetic clipping stiffnesses by solar wind pressure *P is* practically absent ($k \approx 0.1$ - 0.3) and the southward rotation of *the Bz* component *of the* MMP ($k \approx 0.6$ - 0.7), which provided the process of reconnection of magnetic lines of force, is responsible for the development of the geomagnetic storm. A further decrease of *Bz* values led to the weakening of the geomagnetic shield and a decrease of ΔR_{ef} values at the main phase of the storm.

The obtained result that the variations of the geomagnetic clipping stiffness ΔR_{ef} show a high correlation with the plasma parameter β (the ratio of plasma pressure to magnetic pressure), which reaches the maximum value $k = 0.71 \pm 0.12$ at the midlatitude JUNG station, deserves a separate discussion. Recall that a recent paper [Kurazhkovskaya et al., 2021] points to a possibly previously underestimated role of the plasma parameter β in the development of magnetic storms. In [Kurazhkovskaya et al., 2021], we investigated the dynamics of the CB and MMP parameters during the development of 933 geomagnetic storms observed in the period from 1964 to 2010. The similarity of the dynamics of the *Dst-index* and β plasma in the CB was found. The authors [Kurazhkovskaya et al., 2021] attribute this to the fact that the value of the parameter β characterizes the level of space plasma turbulence, which, in turn, can be a significant factor in the development of geomagnetic storms [Antonova, 2002; Borovsky , 2006; D'Amicis, 2010]. In particular, it is suggested in [Kurazhkovskaya et al., 2021] that the achievement of the regime of plasma parameter decrease from the background β = 2 - 2.5 to β = 1 can serve as a trigger for the occurrence of a magnetic storm. Exactly such a drop of β with the beginning of the main phase of the storm can be seen in Fig. 1.

The fact that the change of geomagnetic thresholds ΔR_{ef} correlates most strongly with the *Dst-index* indicates that the ring current plays the main role in controlling the dynamics of the CL

geomagnetic clipping stiffnesses at all stages of the storm. The significant sensitivity to *Dst* is the most typical feature of the interaction of changes in geomagnetic thresholds ΔR_{ef} with the geomagnetosphere, which was noted earlier in [Ptitsyna et al., 2019; Danilova et al., 2023]. The relationship of ΔR_{ef} values with other parameters (magnetic or dynamical) strongly depends on the individual characteristics of a particular geomagnetic perturbation.

6. CONCLUSION

We traced how the changing conditions in the NE and magnetosphere during the evolution of the magnetic storm on March 23-24, 2023, are reflected in the behavior of changes in the CL geomagnetic clipping stiffnesses ΔR_{ef}. We obtained that the largest decrease of ΔR_{ef} values is observed in the main phase at the storm maximum (*Dst* = -163 nTL) and is $\Delta R_{ef} = -0.8$ GV (at Moscow station). In addition, a significant decrease of *R* (~0.5 GV) is recorded at the beginning of the storm as a reaction to the jump-like increase of the NE pressure *P,* which determined the compression of the magnetosphere and the beginning of the storm. This jump of ΔR_{ef} values at all stations was negative. The magnitude of the ΔR_{ef} values and their direction are controlled by the relative contributions of the magnetopause and ring currents, whose effects are opposite [Flüeckiger et al., 1990]. In the case of the studied storm, the effects of the ring current intensification had a predominant influence on the motion of CL particles immediately after the jump-like increase of *P* values. The highest degree of correlation of ΔR_{ef} values was with *Dst* (*k*0.95), indicating that the ring current indeed plays a major role in controlling ΔR_{ef}. In addition, a high degree of correlation with the electromagnetic parameters *B*, *Bz*, *Ey*, and β was found. The dynamic parameters of the CB do not reveal a significant relationship with the values of ΔR_{ef} during the evolution of the studied storm.

Thus, one can see that the dominating factor of changes in the stiffnesses of geomagnetic clipping during the development of the storm on March 23-24 is the ring current, the total effect of the other current systems determines the other obtained correlations. However, it is not possible to determine the contribution of individual current systems because the dynamics of the clipping stiffnesses as a function of the NE and MMP parameters is closely related to the dynamics of the interaction between the NE and the magnetosphere during a strong magnetic storm, which is not yet well understood. The study of the magnetospheric effects of cosmic rays, which can clarify the configuration and dynamics of the Earth's magnetosphere during strong magnetic storms, is a subject of serious attention because this knowledge is essential for understanding the processes in the magnetosphere, for numerical modeling of these processes, and for space weather applications.

CONFLICT OF INTERESTS

The authors declare that there is no conflict of interest.

ACKNOWLEDGEMENTS

We are grateful to an anonymous reviewer who made some very helpful comments.

FUNDING

This work was financed from the budget of the St. Petersburg branch of the N.V. Pushkov Institute of Terrestrial Magnetism, Ionosphere and Radio Wave Propagation of the Russian Academy of Sciences (SPbF IZMIRAN).

REFERENCES

1. Danilova *O.A., Ptitsyna N.G., Tyasto M.I., Sdobnov V.E.* Changes in cosmic ray clipping stiffnesses during the CAWSES II storm on March 8-11, 2012 // Solar-Terrestrial Physics. T. 9. № 2. C. 86-93. 2023.

2. Ermolaev *Yu.I., Nikolaeva N.S., Lodkina I.G., Ermolaev M.Yu.* Catalog of large-scale solar wind phenomena for the period 1976-2000 // Space Research Vol. 47. № 2. C. 99-113. 2009.

3. *Kurazhkovskaya N.A., Zotov O.D., Kline B.I.* Relation of the development of geomagnetic storms with the parameter β of the solar wind // Solar-Terrestrial Physics. T. 7. № 4. C. 25-34. 2021.

4. Ptitsyna *N.G., Danilova O.A., Tyasto M.I., Sdobnov V.E.* Influence of the solar wind parameters and geomagnetic activity on the variations of cosmic ray clipping stiffness during strong magnetic storms // Geomagnetism and Aeronomy. T. 59. № 5. C. 569-577. 2019.

5. *Adriani O., Barbarino G.C., Bazilevskaya G.N. et al.* PAMELA's measurements of geomagnetic cutoff variations during the December 14, 2006 storm // Space weather. V. 14. № 3. P. 210-220. 2016.

6. Akasofu *S.I.* The magnetospheric currents: An introduction. In T. A. Potemra (Ed.), Magnetospheric currents // Geophysical MonographSeries. Washington, DC: American Geophysical Union. V. 28. P. 29-48. 1984.

7. *Alexeev I.I., Kalegaev V.V., Belenkaya E.S., Bobrovnikov S.Y., Feldstein Ya.I., and Gromova L.I.* Dynamic Model of the Magnetosphere: Case Study for January 9-12,1997 // J. Geophys. Geophys. Res. V. 106. P. 25683-25694. 2001.

8. Antonova *E.E.* Magnetostatic equilibrium and turbulent transport in Earth's magnetosphere: A review of experimental observation data and theoretical approaches // International Journal of Geomagnetism and Aeronomy. V. 3. № 2. P. 117-130. 2002.
9. Belov *A., Baisultanova L., Eroshenko E., Mavromichalaki H., Yanke V., Pchelkin V., Plainaki C., Mariatos G.* Magnetospheric effects in cosmic rays during the unique magnetic storm on November 2003 // *J.* Geophys. Geophys. Res. V. 110. A09S20. 2005.
10. *Belov S.M., Zobnin G.I., and Yanke V.G.* Program for calculating the geomagnetic cutoff rigidity of cosmic rays and the trajectories of their motion // Bull. Russ. Acad. Sci.: Phys. V. 85. № 11. P. 1297-1301. 2021.
11. *Borovsky J.E., Denton M.H.* Differences between CMEdriven storms and CIR-driven storms // J. Geophys. Geophys. Res. V. 111. Iss. A7. A07S08. 2006.
12. Castillo *Y., Pais M.A., Fernandes J., Ribeiro P., Morozova A.L.* Geomagnetic activity at Northern Hemisphere's mid-latitude ground stations: How much can be explained using Ts05 model // Journal of Atmospheric and Solar-Terrestrial Physics. V. 165-166. P. 38-53. 2017.
13. D*'Amicis R., Bruno R., Bavassano B.* Geomagnetic activity driven by solar wind turbulence // JASR. V. 46. P. 514-520. . 2010. https://doi.org/10.1016/j.asr.2009.08.031
14. Dorman *L.I.* Elementary particle and cosmic ray physics. Elsevier. New *York*. 456 p. 1963.
15. *Dungey J.W.* Interplanetary magnetic field and the auroral zones / Phys Rev Lett. V. 6. P. 47-48. 1961.
16. *Dubyagin S., Ganushkina N., Kubyshkina M., Liemohn M.* Contribution from different current systems to SYM and ASY midlatitude indices // J. Geophys. Geophys. Res. Space Phys. V 119. P. 7243-7263. 2014.
17. *Flückiger E.O., Smart D.F., Shea M.A.* Determination of the strength of the ring and the magnetopause currents during the initial phase of geomagnetic storm using cosmic ray data // J. Geophys. Geophys. Res. V. 95 (A2). P. 1113-1118. 1990. https://doi.org/10.1029/ JA095iA02p01113
18. *Ganushkina N.Y., Liemohn M.W., Dubyagin S.* Current systems in the Earth's magnetosphere // Reviews of Geophysics. V. 56. P 309-332. 2018. https://doi.org/10.1002/2017RG000590
19. Gosling *J.T.* The solar flare myth // J. Geophys. Res. Space Physics. V. 98. № A11. 18937-18949. 1993. https://doi.org/10.1029/93JA01896
20. Gonzalez *W.D., Tsurutani B.T.* Criteria of Interplanetary Parameters Causing Intense Magnetic Storms (Dst < -100 nT) // Planetary Space Science V. 35. P. 110-1109. 1987. https://doi.org/10.1016/0032-0633(87)

21. Gonzalez *W.D., Tsurutani B.T., Clúa de Gonzalez A.L.* Interplanetary origin of geomagnetic storms // Space Science Reviews. V. 88. № 3. P. 529-562. 1999.

22. *Gromova, L.I., Kleimenova, N.G., Gromov, S.V., K. K. Kanonidi, V. G. Petrov, L. M. Malysheva.* Intensive substorms during the main phase of the magnetic storm on March 23-24, 2023 // Geomagn. Aeron. V. 64. P. 881-889. 2024 .

23. *Kalegaev V.V., Ganushkina N.Yu., Pulkkinen T.I., Kubyshkina M.V., Singer H.J., Russell C.T.* Relation between the Ring Current and the Tail Current During Magnetic Storms // Ann. Geophys. V. 26. No. 2. P. 523-533. 2005.

24. *Kalegaev V.V.* Dynamic Geomagnetic Field Models // Geomagnetism and Aeronomy. V. 51. No. 7. P. 855-865. 2011.

25. Kress *B.T., Mertens C.J., Wiltberger M.* Solar energetic particle cutoff variations during the October 29-31, 2003 geomagnetic storm // Space Weather. V. 8. S05001. 2010. https://doi.org/10.1029/2009SW000488

26. Kress *B. T., Hudson M. K., Perry K. L., Slocum P. L.* Dynamic modeling of geomagnetic cutoff for the 23-24 November2001 solar energetic particle event // Geophys. Res. Lett. V. 31. L04808. 2004.

27. Kress *B.T., Hudson M.K., Selesnick R.S., Mertens C.J., Engel M.* Modeling geomagnetic cutoffs for space weather applications // J. Geophys. Geophys. Res. Space Physics. V. 120. No. 7. P. 5694-5702. 2015. https://doi.org/10.1002/2014JA020899

28. *McCracken K.G., Rao U.R., Shea M.A.* The trajectories of cosmic rays in a high degree simulation of the geomagnetic field // M.I.T. Tech. Rep. 77. Lab. for Nucl. Sci. and Eng., Mass. Inst. of Technol. Cambridge. 1962.

29. *Ptitsyna N. G., Danilova O.A., Tyasto M.I, Sdobnov V.E.* Cosmic ray cutoff rigidity governing by solar wind and magnetosphere parameters during the 2017 Sep 6-9 solar-terrestrial event // Journal of Atmospheric and Solar-Terrestrial Phys. V. 246. Article Number 106067. 2023. https://doi.org/10.1016/j.jastp.2023.106067

30. Richardson *I.G.* Solar wind stream interaction regions throughout the heliosphere // Living Rev Sol Phys. V. 15. No. 1. P.1-95. 2018.

31. Russell *C. T.* Reconnexion, in Physics of Solar Planetary Environments / Proceedings of the International Symposium on Solar-Terrestrial Physics. June 7-18. 1976. Boulder. Colorado V.II, edited by D. J. Williams. P. 526-540. AGU. Washington D. C. 1976.

32. Shea *M.A., Smart D.F., McCracken K.G.* A study of vertical cutoff rigidities using sixth degree simulations of the geomagnetic field // J. Geophys. Geophys. Res. V. 70. P. 4117-4130. 1965.

33. Shimazu *H.* Solar proton event and proton propagation in the Earth's magnetosphere // J. Nat. Natl. Inst. Inf. Commun.Technol. V. 56. No. 1-4. P. 191-199. 2009.
34. *Störmer C*. The Polar Aurora // London: Oxford University Press. Quarterly Journal of the Royal Meteorological Society: V. 82, Iss. 351. P. 115-115. 1956. ttps://doi.org/10.1002/qj.49708235123.
35. Tahir *A., Wu F., Shah M, Amory-Mazaudier C., Jamjareegulgarn P., Verhulst T.G.W., Ameen M.A.* Multi-Instrument Observation of the Ionospheric Irregularities and Disturbances during the 23-24 March 2023 Geomagnetic Storm // Remote Sens. V. 16. № 9. P. 1594-1621. 2024 .https://doi.org/10.3390/rs16091594
36. Teng *W., Su Y., Ji H., Zhan Q.* Unexpected major geomagnetic storm caused by faint eruption of a solar transequatorial flux rope // Nature Communications. V. 15. P. 9198-9214. 2024 https://doi.org/10.1038/s41467-024-53538-1.
37. Tsyganenko *N.A., Singer H.J., Kasper J.C.* Storm-time distortion of the inner magnetosphere: How severe can it get? // J. Geophys. Res. V. 108 (A5). P. 1209-1215. 2003.
38. *Tyssøy H.N., Stadsnes J.* Cutoff latitude variation during solar proton events: Causes and consequences. J. Geophys.Res.Space Physics. V. 120. P. 553-563. 2014.
39. https://kauai.ccmc.gsfc.nasa.gov/CMEscoreboard/PreviousPredictions/2023.

Table 1. Cosmic ray stations

N	Station name	International code	Geographic latitude	Geographic longitude	R_c
1	Kingston (Australia)	KGSN	42.99° S	147.29° E	1.9
2	Moscow (Russia)	MOSC	55.47° N	37.32° E	2.08
3	Irkutsk (Russia)	IRKT	52.47° N	104.03° E	3.13
4	Jungfrau (Switzerland)	JUNG	46.55° N	7.98° E	4.51
5	Almaty (Kazakhstan)	AATA	43.25° N	76.92° E	5.21
6	Athens (Greece)	ATHN	37.97° N	23.72° E	8.48
7	ESOI (Israel)	ESOI	33.30° N	35.80° E	10.73

Table 2. Correlation coefficients k between ΔR_{ef} and parameters (P) of geomagnetic activity, CB and IMF

Π	ESOI	ATHN	AATA	JUNG	IRKT	MOSC	KGSN
Dst	0.94±0.04	0.94±0.05	0.95±0.05	0.96±0.05	0.95±0.06	0.93±0.09	0.93±0.09
K_p	−0.75±0.07	−0.75±0.10	−0.77±0.11	−0.74±0.11	−0.79±0.13	−0.80±0.14	−0.80±0.15
E_y	−0.57±0.09	−0.65±0.11	−0.59±0.13	−0.64±0.13	−0.62±0.17	−0.68±0.18	−0.64±0.19
B_z	0.59±0.09	0.67±0.11	0.61±0.13	0.66±0.13	0.65±0.16	0.70±0.17	0.66±0.18
B_y	0.32±0.10	0.35±0.14	0.36±0.16	0.35±0.16	0.38±0.20	0.29±0.23	0.36±0.23
B	−0.70±0.08	−0.69±0.11	−0.69±0.12	−0.72±0.12	−0.68±0.16	−0.74±0.16	−0.68±0.18
V	0.45±0.10	0.42±0.13	0.47±0.15	0.44±0.15	0.44±0.19	0.38±0.22	0.43±0.22
N	−0.33±0.10	−0.29±0.14	−0.34±0.16	−0.22±0.16	−0.42±0.19	−0.31±0.23	−0.46±0.22
P	−0.14±0.10	−0.12±0.15	−0.17±0.16	−0.05±0.17	−0.25±0.21	−0.17±0.24	−0.30±0.23
β	0.63±0.09	0.65±0.11	0.63±0.13	0.71±0.12	0.57±0.17	0.70±0.17	0.57±0.20

Figure captions

Fig. 1. Variations of geomagnetic clipping stiffness and solar wind parameters, MMPs, and geomagnetic activity indices during the storm of March 23-24, 2023. Vertical lines indicate the main phase of the storm.

Fig. 2. Variations of geomagnetic thresholds ΔR_{ef} for the studied stations during the storm evolution on September 23-24, 2023. a - *Dst-index*; b - ΔR_{ef}. The ΔR_{ef} curves are arranged from top to bottom in the order of increasing CL station latitude (decreasing threshold stiffnesses $R_{c)}$. The vertical lines mark the main phase of the storm, as in Fig. 1.

Fig. 3. Diagram of geoeffective ($\left| k \right| \geq 0.45$) correlations of the values of variations in the stiffnesses of geomagnetic clipping ΔR_{ef} stiffnesses with interplanetary and geomagnetic parameters.

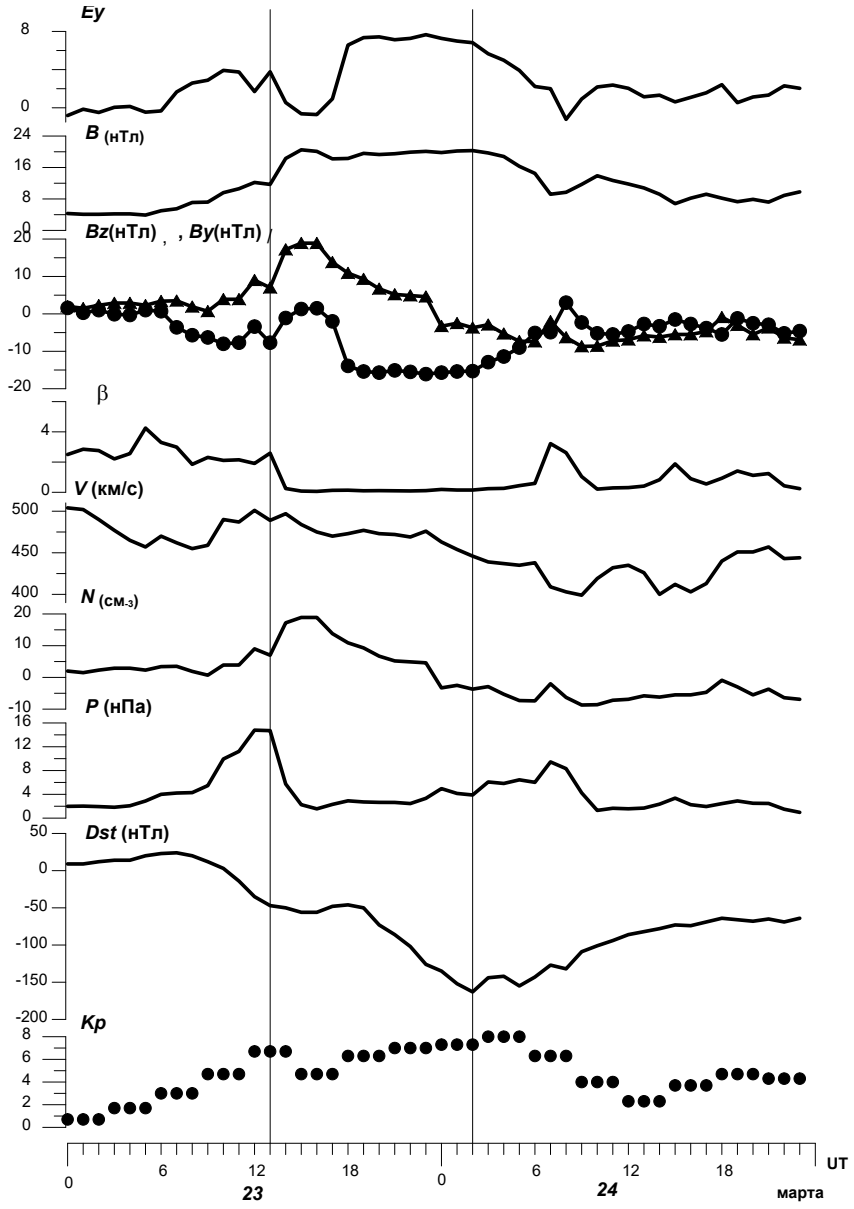
Ey
8
0
B (нТл)
24
16
8
0
Bz(нТл) , By(нТл)
20
10
0
-10
-20
β
4
0
V (км/с)
500
450
400
N (см-3)
20
10
0
-10
P (нПа)
16
12
8
4
0
Dst (нТл)
50
0
-50
-100
-150
-200
Kp
8
6
4
2
0
0
6
12
18
0
6
12
18
UT
23
24
марта

Fig. 1.

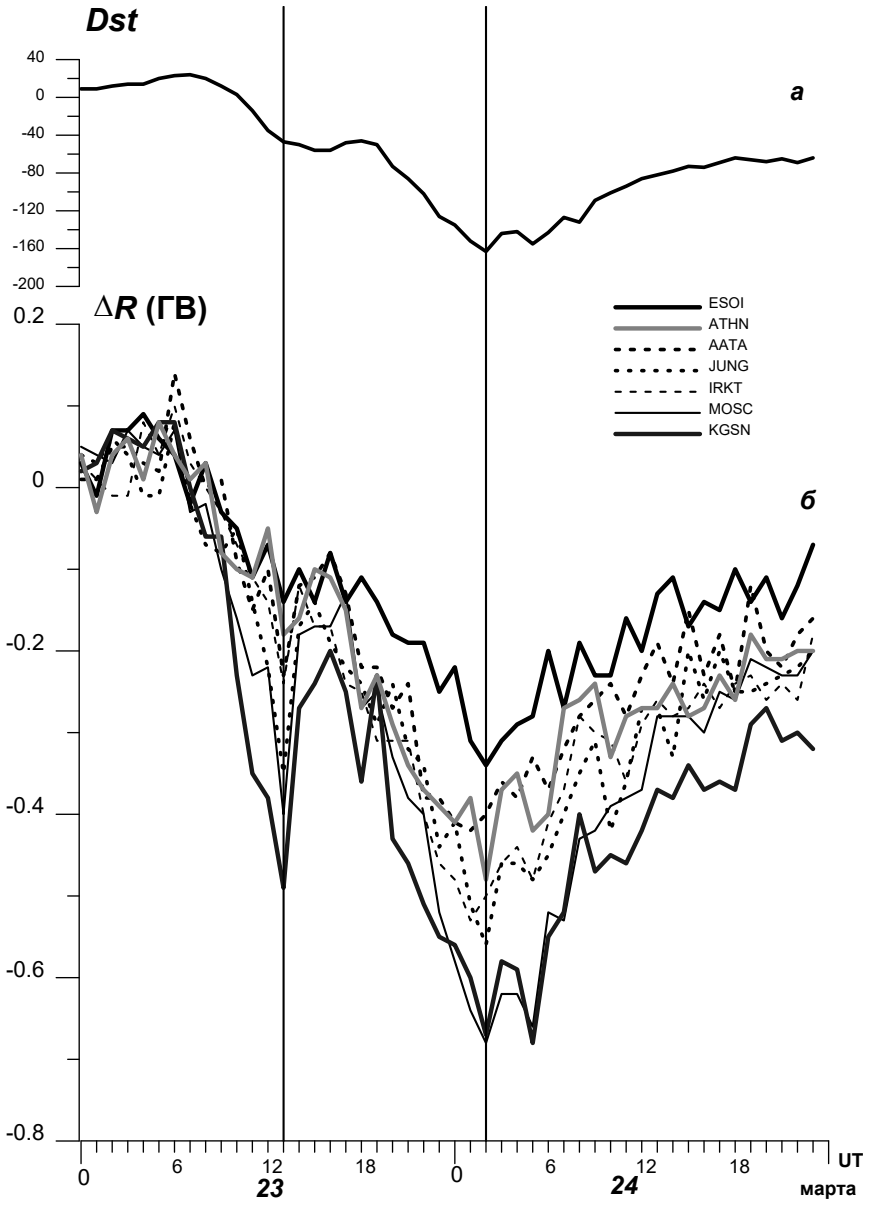
Dst
40
0
-40
-80
-120
-160
-200
а
ΔR (ГВ)
0.2
0
-0.2
-0.4
-0.6
-0.8
ESOI
ATHN
AATA
JUNG
IRKT
MOSC
KGSN
б
0
6
12
18
0
6
12
18
UT
23
24
марта

Fig. 2.

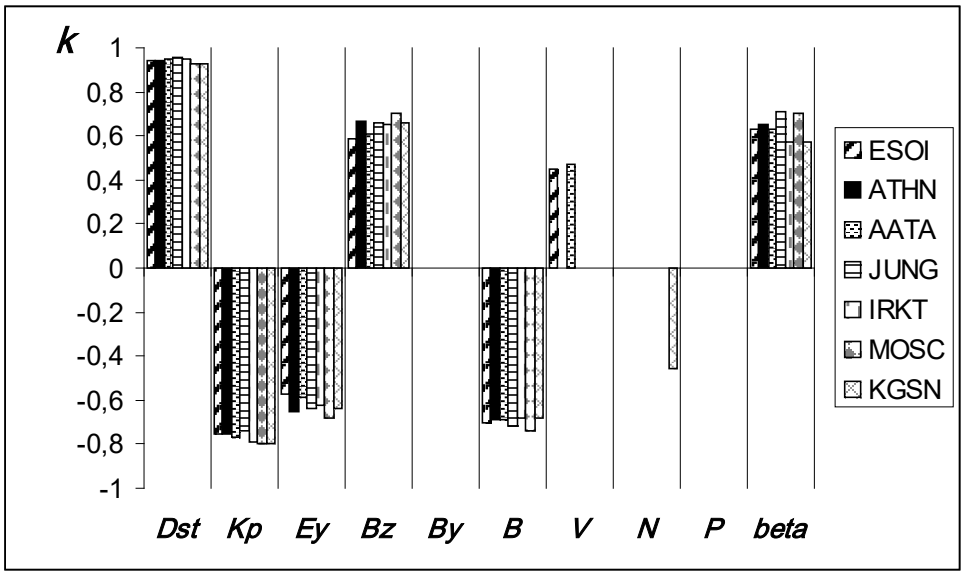
k
1
0,8
0,6
0,4
0,2
0
-0,2
-0,4
-0,6
-0,8
-1
Dst
Kp
Ey
Bz
By
B
V
N
P
beta
ESOI
ATHN
AATA
JUNG
IRKT
MOSC
KGSN

Fig. 3.